Unexpected neutron/proton ratio and isospin effect in low-energy antiproton-induced reactions

Zhao-Qing Feng*

Institute of Modern Physics, Chinese Academy of Sciences, Lanzhou 730000, People's Republic of China

(Received 23 January 2017; published 13 September 2017)

The inclusive spectra of pre-equilibrium nucleons produced in low-energy antiproton-nucleus collisions are thoroughly investigated within the the Lanzhou quantum molecular dynamics transport approach for the first time. The reaction channels of elastic scattering, annihilation, charge exchange, and inelastic processes in antibaryon-baryon, baryon-baryon, and meson-baryon collisions have been implemented in the model. The unexpected neutron to proton yield ratios are caused from the isospin effects of pion-nucleon collisions and the symmetry energy. It is found that the π^--neutron collisions enhance the neutron emission in the antiproton annihilation in a nucleus. A soft symmetry energy with the stiffness of $\gamma_s = 0.5$ at subsaturation densities is constrained from the available data of the neutron/proton spectra.

DOI: 10.1103/PhysRevC.96.034607

I. INTRODUCTION

Since the first evidence of antiprotons was found in 1955 at Berkeley in collisions of protons on copper at the energy of 6.2 GeV by Chamberlain *et al.* [1], the secondary beams of antiprotons were produced at many laboratories, such as CERN, BNL, KEK, etc. [2–5]. The stochastic cooling method provides the possibility for storing the antiprotons produced in proton-nucleus collisions. The particles $W^{\pm}$ and Z^0 were found for the first time with the high-energy protons colliding with the stored antiprotons at CERN [6]. On the other hand, the antiproton-nucleus collisions are connected to many interesting issues, i.e., charmonium physics, strangeness physics, antiprotonic atom, symmetry, in-medium properties of hadrons, cold quark-gluon plasma, highly excited nuclei, etc. [7,8]. Recently, the antiproton-antiproton interaction was investigated by the STAR collaboration in relativistic heavy-ion collisions [9].

In past decades, the nuclear reactions induced by antiprotons were investigated with the facilities of the low-energy antiproton ring (LEAR) at CERN [10], the National Laboratory for High Energy Physics at KEK [11], and the BNL Alternating Gradient Synchrotron accelerator [12]. A number of interesting phenomena were observed, e.g., the delayed fission from the decay of hypernuclei in antiproton annihilations on heavy nuclei [13], the unexpected enhancement of the Λ/K_S^0 ratio [14], the decay mode of highly excited nuclei, etc. [15,16]. The low-energy antiprotons are usually annihilated at the nucleus surface because of the large absorption cross section. A huge amount of annihilation energy is available to produce 2–6 pions [17,18]. The subsequent processes are complicated and also associated with the multiple pion-nucleon interaction, which results in the fragmentation of the target nucleus and the pre-equilibrium emissions of complex particles [19,20].

The dynamics of the antiproton-nucleus collisions is more complicated in comparison to hadron (proton, π, K, etc.)-induced reactions and to heavy-ion collisions, in which the particles produced in the annihilation of the antiproton in a nucleus are coupled to the subsequent collisions with the surrounding nucleons. The dynamics of antiproton-nucleus collisions is complicated, which is associated with the mean-field potentials of hadrons in nuclear medium, and also coupled to a number of reaction channels, i.e., the annihilation channels, the charge-exchange reaction, and elastic and inelastic collisions. There have been several approaches for describing the nuclear dynamics induced by antiprotons, e.g., the intranuclear cascade model [21], the kinetic approach [22], the Giessen Boltzmann-Uehling-Uhlenbeck transport model [23], the statistical multifragmentation model [24] and the Lanzhou quantum molecular dynamics (LQMD) approach [25]. Part of the experimental data can be understood within these models.

A more localized energy is deposited in the nucleus with an excitation energy of several hundreds of MeV. The hot nucleus proceeds to the explosive decay via the multifragmentation process or the sequential particle evaporation. On the other hand, the collisions of the antiproton and secondary particles with the surrounding nucleons lead to pre-equilibrium particle emissions, which are related to the scattering cross sections of each reaction channel, antiproton-nucleon interaction, particle-nucleon potential, and density profile of the target nucleus. The unexpected large neutron yields produced by stopped antiprotons in nuclei were reported in the LEAR experiments [26,27]. This phenomenon has been puzzling physicists for several decades [28]. In this work, the pre-equilibrium nucleon emissions and the neutron/proton (n/p) spectra in antiproton-induced nuclear reactions are investigated within the LQMD transport model.

II. BRIEF DESCRIPTION OF THE LQMD MODEL

In the LQMD model, the dynamics of resonances of hyperons and mesons with a mass below 2 GeV is coupled to the hadron-hadron collisions, antibaryon-baryon annihilations, and decays of resonances [25,29]. The temporal evolutions of all particles are described by Hamilton's equations of motion under self-consistently generated mean-field potentials. A Hamiltonian of nucleons and nucleonic resonances is constructed from the Skyrme energy-density functional. The dynamics of hyperons, antibaryons, and mesons is described with the effective interactions based on the relativistic covariant theories. The interaction potential of the nucleonic system is evaluated from the energy-density functional of

*fengzhq@impcas.ac.cn

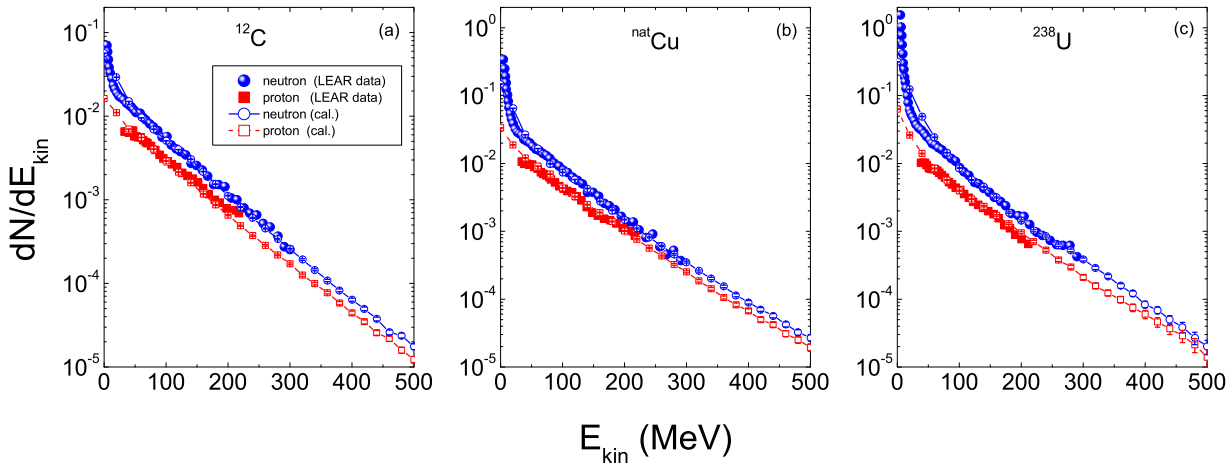

FIG. 1. Kinetic energy spectra of neutrons and protons produced in antiproton annihilations on carbon, copper, and uranium at an incident momentum of 200 MeV/c and compared with the available data at the LEAR facility [27].

$U_{\rm loc} = \int V_{\rm loc}[\rho(\mathbf{r})]d\mathbf{r}$, with

$$V_{\rm loc}(\rho) = \frac{\alpha}{2}\frac{\rho^2}{\rho_0} + \frac{\beta}{1+\gamma}\frac{\rho^{1+\gamma}}{\rho_0^{\gamma}} + E_{\rm sym}^{\rm loc}(\rho)\rho\delta^2 + \frac{g_{\rm sur}}{2\rho_0}(\nabla\rho)^2 + \frac{g_{\rm sur}^{\rm iso}}{2\rho_0}[\nabla(\rho_n-\rho_p)]^2, \quad (1)$$

where ρ_n, ρ_p, and $\rho = \rho_n + \rho_p$ are the neutron, proton, and total densities, respectively, and $\delta = (\rho_n - \rho_p)/(\rho_n + \rho_p)$ is the isospin asymmetry of the baryonic matter. The parameters α, β, and γ are taken to be -226.5 MeV, 173.7 MeV, and 1.309, respectively. The set of the parameters gives the compression modulus of $K = 230$ MeV for isospin symmetric nuclear matter at the saturation density ($\rho_0 = 0.16$ fm^{-3}). The surface coefficients $g_{\rm sur}$ and $g_{\rm sur}^{\rm iso}$ are taken to be 23 and -2.7 MeV fm^2, respectively. The third term contributes the symmetry energy being of the form $E_{\rm sym}^{\rm loc} = \frac{1}{2}C_{\rm sym}(\rho/\rho_0)^{\gamma_s}$. The parameter $C_{\rm sym}$ is taken as the value of 38 MeV. The γ_s could be adjusted to get a suitable case by constraining the isospin observables, e.g., the values of 0.5, 1, and 2 being the soft, linear, and hard symmetry energy, respectively. Combining the kinetic energy from the isospin difference of nucleonic Fermi motion, the three kinds cross at a saturation density with a value of 31.5 MeV. The mean-field potential of the antinucleon is constructed from the G-parity transformation of nucleon self-energies with a scaling approach [25,30], which leads to a strength of the optical potential of $V_{\overline{N}} = -164$ MeV at normal nuclear density.

The annihilation reactions in antibaryon-baryon collisions are described by a statistical model with SU(3) symmetry of pseudoscalar and vector mesons [31], which considers possible combinations with the final state from two to six mesons [32]. Pions as the dominant products in antibaryon-baryon annihilation contribute the energy deposition into the target nucleus via the pion-nucleon collisions, which leads to the emission of pre-equilibrium particles, fission, the evaporation of nucleons and light fragments, etc. The cross section of pion-nucleon scattering is evaluated with the Breit-Wigner formula in the form of [33]

$$\sigma_{\pi N\to R}(\sqrt{s}) = \sigma_{\rm max}|\mathbf{p}_0/\mathbf{p}|^2\frac{0.25\Gamma^2(\mathbf{p})}{0.25\Gamma^2(\mathbf{p}) + (\sqrt{s}-m_0)^2}, \quad (2)$$

where $\mathbf{p}$ and $\mathbf{p}_0$ are the momenta of pions at energies of $\sqrt{s}$ and m_0, respectively, with m_0 being the centroid of resonance mass, e.g., 1.232 GeV for $\Delta(1232)$. The maximum cross section $\sigma_{\rm max}$ is taken by fitting the available experimental data and is satisfied to the squares of the Clebsch-Gordan coefficients [34], i.e., 200, 133.3, and 66.7 mb for $\pi^+ + p \to \Delta^{++}$, $\pi^0 + p \to \Delta^+$, and $\pi^- + p \to \Delta^0$, respectively.

III. RESULTS AND DISCUSSION

The emission of fast nucleons produced in antiproton-induced reactions is a significant observable in understanding the energy deposition, antiproton-nucleon, and meson-nucleon interactions in nuclear medium. Shown in Fig. 1 is the kinetic energy distributions of neutrons and protons produced in antiproton annihilations on ^{12}C, ^{nat}Cu, and ^{238}U at an incident momentum of 200 MeV/c and compared with the available data at the LEAR facility [27]. Overall, the spectra can be nicely understood within the LQMD transport model. The pre-equilibrium nucleons in the model are constructed with a coalescence approach, in which nucleons at the freeze-out stage in phase space are considered to belong to one cluster with the relative momentum being smaller than P_0 and with the relative distance being smaller than R_0 (here $P_0 = 200$ MeV/c and $R_0 = 3$ fm). On the other hand, part of the nucleons are from the decay of the primary fragments after the antiproton annihilation, which contributes to the nucleon yields within the kinetic energy below 20 MeV. The deexcitation of the primary fragments is assumed to be isolated without rotation (zero angular momentum) and is evaluated with the statistical code GEMINI [35]. The nucleon yields are weakly influenced by varying the coalescence parameters. The antiproton-nucleus systems evolve to 500 fm/c for judging the free nucleon formation. It should be noticed that the neutrons are preferable to be emitted in comparison to the protons. The energy deposition in antiproton-induced reactions is more explosive than in the case of Fermi-energy heavy-ion collisions [36,37], which leads to energetic nucleon emission. In the annihilation of an antiproton in a nucleus, pions are the dominant products. For example, the multiplicities of π^- and π^+ on the target

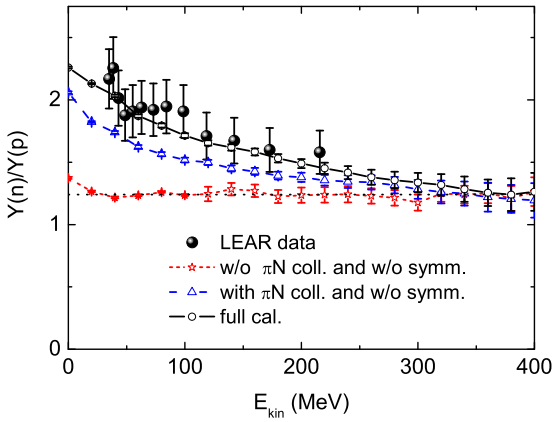

FIG. 2. Impacts of πN absorption and symmetry energy on the yield ratios of neutrons to protons in the $\overline{p}+{}^{65}$Cu reaction at 200 MeV/c and the experimental data with the stopped $\overline{p}$ on $^{\text{nat}}$Cu [27].

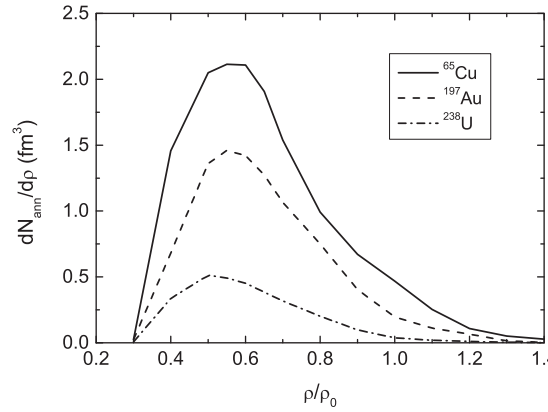

FIG. 3. Nuclear density profiles at which antiprotons are annihilated on the targets of ^{65}Cu, ^{197}Au, and ^{238}U.

of ^{12}C are 1.5 and 0.6, respectively. On the other hand, the larger elastic scattering cross sections in the $\pi^- n$ reactions [the maximal value being 200 mb at the Δ-resonance energy ($E = 0.19$ GeV, $p = 0.298$ GeV/c)], in comparison to the $\pi^- p$ collisions (25 mb at the pion energy of 0.19 GeV), enhance the $\pi^- n$ collision probabilities and are favorable to neutron emissions in the low-energy antiproton-induced reactions even on the isospin symmetric target of ^{12}C. For neutron-rich targets such as ^{238}U, the difference in neutron and proton yields is more pronounced.

The ratio spectra of the isospin particles produced in heavy-ion collisions are related to the isospin-dependent cross sections and interaction potentials [29,38,39]. The kinetic energy distributions of the n/p ratio and the double n/p ratio in isotopic nuclear reactions have been used for constraining the density dependence of symmetry energy. The yield ratios of neutrons and protons are complicated in low-energy antiproton-induced reactions, which are related to antiproton-nucleon scattering, annihilation in antinucleon-nucleon collisions, and pion-nucleon scattering. The experimental n/p spectra in pion- and proton-nucleus collisions were nicely explained by the intranuclear cascade model [28]. The kinetic energy spectra of the n/p ratio in antiproton-induced reactions cannot be understood by the model. The n/p ratio in antiproton-nucleus collisions has been further investigated within the LQMD transport model, in which the isospin effects associated with the pion and nucleon dynamics are treated self-consistently. The yield ratios of neutrons and protons produced in the $\overline{p}+{}^{65}$Cu collisions at an incident momentum of 200 MeV/c are strongly constrained by the pion-nucleon collisions and symmetry energy as shown in Fig. 2. Here, the linear symmetry energy with $\gamma_s = 1$ is chosen. Pions, as the dominant products in the antiproton annihilation in a nucleus, heat the nucleus with an excitation around 300 MeV and contribute to the nucleon removal from the target nucleus [40,41]. A flat n/p spectrum appears once removed from the pion-nucleon collisions and is close to the mean value (1.24) of the target nucleus. The final multiplicities of π^- and π^+ in collisions of antiprotons on ^{65}Cu are 1.53 and 0.94, respectively. The $n\pi^-$ scattering enhances the neutron emission, in particular at the kinetic energies below 150 MeV. The symmetry energy further increases the n/p ratio because of its repulsive contribution to neutrons in neutron-rich matter. Both the pion-nucleon collisions and the symmetry energy dominate the n/p spectra.

The stiffness of symmetry energy impacts the isospin dynamics in heavy-ion collisions. However, the nuclear density of isospin particle emissions varies in the evolution of nucleus-nucleus collisions. On the other hand, the rotation of a colliding system complicates the emission angles of isospin particles. The density profiles of antiprotons annihilated on nuclei are shown Fig. 3. It is of interest that the antiprotons are mainly annihilated in the density domain of 0.4–0.8 ρ_0. The nucleons are emitted around the densities of 0.08–0.1 fm^{-3} after interacting with pions. The nucleons from the subsequential processes due to the secondary collisions are evaporated from the excited primary fragments with the less kinetic energy. Therefore, the n/p ratio with the kinetic energies above 50 MeV directly provides the symmetry energy information at subsaturation densities. Shown in Fig. 4 is the kinetic energy spectra in antiproton-induced reactions on ^{12}C, $^{\text{nat}}$Cu, ^{197}Au, and ^{238}U with the soft ($\gamma_s = 0.5$) and hard ($\gamma_s = 2$) symmetry energies, respectively. The dashed lines represent the mean

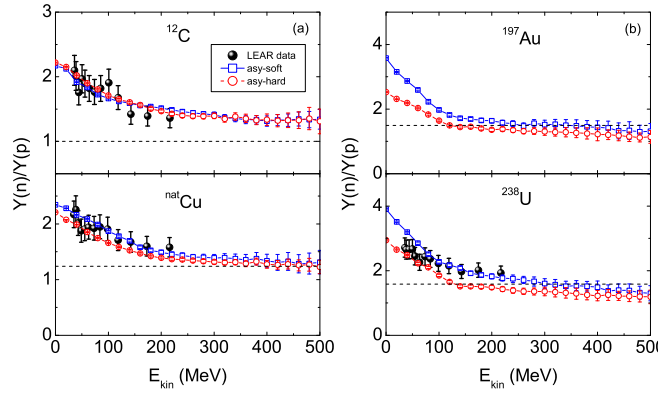

FIG. 4. The n/p ratios in antiproton-induced reactions on ^{12}C, $^{\text{nat}}$Cu, ^{197}Au, and ^{238}U with different stiffnesses of symmetry energies and compared with the LEAR data [27].

n/p values of the target nuclei. Calculations are performed at an antiproton momentum of 200 MeV/c. I have checked that the spectra are insensitive to the incident energy. It is obvious that the difference of the stiffness of symmetry energy is pronounced in the neutron-rich nuclei. The n/p ratio is enhanced with softening of the symmetry energy. Overall, the available data at the LEAR facility [27] are reproduced with the soft symmetry energy. Different from the Fermi-energy heavy-ion collisions [37], the isospin effect appears at kinetic energies below 200 MeV. The kinetic energy spectra of the n/p ratio in the antiproton-induced reactions are expected to be further measured at PANDA (Antiproton Annihilation at Darmstadt, Germany) in the near future experiments.

IV. CONCLUSIONS

In summary, the kinetic energy spectra of the n/p ratio produced in the antiproton annihilation in the nucleus have been puzzling for several decades. The structure is quite different with the proton (pion)-induced reactions and also with the heavy-ion collisions. The available data from the LEAR facility are nicely explained with the LQMD transport model for the first time. It is found that the $n\pi^-$ scattering and the symmetry energy increase the neutron emission and lead to the enhancement of the n/p ratio, in particular in the domain of kinetic energies below 200 MeV because of the larger $n\pi^-$ collision probability. The soft symmetry energy with a stiffness of $\gamma_s = 0.5$ is constrained from the LEAR data.

ACKNOWLEDGMENTS

This work was supported by the National Natural Science Foundation of China (Projects No. 11722546 and No. 11675226) and the Chinese Academy of Sciences (Grant No. QYZDJ-SSW-SLH041).

[1] O. Chamberlain, E. Segrè, C. Wiegand, and T. Ypsilantis, Phys. Rev. **100**, 947 (1955).
[2] O. Chamberlain, D. V. Keller, R. Mermod, E. Segrè, H. M. Steiner, and T. Ypsilantis, Phys. Rev. **108**, 1553 (1957).
[3] L. E. Agnew *et al.*, Phys. Rev. **118**, 1371 (1960).
[4] LEAR Design Study Team, Design Study of a Facility for Experiments with Low Energy Antiprotons (LEAR), CERN Report CERN/PS/DL 80-7, 1980.
[5] J. Eades and F. J. Hartmann, Rev. Mod. Phys. **71**, 373 (1999).
[6] UA1 Collaboration, Phys. Lett. B **122**, 103 (1983); **129**, 273 (1983).
[7] M. Amoretti *et al.*, Nature (London) **419**, 456 (2002).
[8] J. Rafelski, Phys. Lett. B **91**, 281 (1980); **207**, 371 (1988).
[9] STAR Collaboration, Nature **527**, 345 (2015).
[10] F. Goldenbaum *et al.*, Phys. Rev. Lett. **77**, 1230 (1996); U. Jahnke, W. Bohne, T. von Egidy, P. Figuera, J. Galin, F. Goldenbaum, D. Hilscher, J. Jastrzebski, B. Lott, M. Morjean, G. Pausch, A. Péghaire, L. Pienkowski, D. Polster, S. Proschitzki, B. Quednau, H. Rossner, S. Schmid, and W. Schmid, *ibid.* **83**, 4959 (1999).
[11] K. Miyano, Y. Noguchi, M. Fukawa, E. Kohriki, F. Ochiai, T. Sato, A. Suzuki, K. Takahashi, Y. Yoshimura, N. Fujiwara, S. Noguchi, S. Yamashita, and A. Ono, Phys. Rev. Lett. **53**, 1725 (1984).
[12] T. Lefort, K. Kwiatkowski, W.-c. Hsi, L. Pienkowski, L. Beaulieu, B. Back, H. Breuer, S. Gushue, R. G. Korteling, R. Laforest, E. Martin, E. Ramakrishnan, L. P. Remsberg, D. Rowland, A. Ruangma, V. E. Viola, E. Winchester, and S. J. Yennello, Phys. Rev. Lett. **83**, 4033 (1999).
[13] J. P. Bocquet *et al.*, Phys. Lett. B **182**, 146 (1986); **192**, 312 (1987).
[14] K. Miyano, Y. Noguchi, Y. Yoshimura, M. Fukawa, F. Ochiai, T. Sato, R. Sugahara, A. Suzuki, K. Takahashi, N. Fujiwara, S. Noguchi, S. Yamashita, A. Ono, M. Chikawa, O. Kusumoto, and T. Okusawa, Phys. Rev. C **38**, 2788 (1988).
[15] T. von Egidy, H. Daniel, F. J. Hartmann, W. Kanert, E. F. Moser, Ye. S. Golubeva, A. S. Iljinov, and J. J. Reidy, Z. Phys. A **335**, 451 (1990).
[16] J. Jastrzębski, W. Kurcewicz, P. Lubiński, A. Grabowska, A. Stolarz, H. Daniel, T. von Egidy, F. J. Hartmann, P. Hofmann, Y. S. Kim, A. S. Botvina, Y. S. Golubeva, A. S. Iljinov, G. Riepe, and H. S. Plendl, Phys. Rev. C **47**, 216 (1993).
[17] P. Hofmann, A. S. Iljinov, Y. S. Kim, M. V. Mebel, H. Daniel, P. David, T. von Egidy, T. Haninger, F. J. Hartmann, J. Jastrzebski, W. Kurcewicz, J. Lieb, H. Machner, H. S. Plendl, G. Riepe, B. Wright, and K. Ziock, Phys. Rev. C **49**, 2555 (1994).
[18] P. Lubiński, A. Grochulska, T. von Egidy, K. Gulda, F. J. Hartmann, J. Jastrzebski, W. Kurcewicz, L. Pienkowski, A. Stolarz, and A. Trzcińska, Phys. Rev. C **66**, 044616 (2002).
[19] Y. S. Kim, A. S. Iljinov, M. V. Mebel, P. Hofmann, H. Daniel, T. von Egidy, T. Haninger, F. J. Hartmann, H. Machner, H. S. Plendl, and G. Riepe, Phys. Rev. C **54**, 2469 (1996).
[20] B. Lott, F. Goldenbaum, A. Böhm, W. Bohne, T. von Egidy, P. Figuera, J. Galin, D. Hilscher, U. Jahnke, J. Jastrzebski, M. Morjean, G. Pausch, A. Péghaire, L. Pienkowski, D. Polster, S. Proschitzki, B. Quednau, H. Rossner, S. Schmid, and W. Schmid, Phys. Rev. C **63**, 034616 (2001).
[21] J. Cugnon, P. Deneye, and J. Vandermeulen, Nucl. Phys. A **500**, 701 (1989); Phys. Rev. C **41**, 1701 (1990).
[22] C. M. Ko and R. Yuan, Phys. Lett. B **192**, 31 (1987).
[23] A. B. Larionov, I. A. Pshenichnov, I. N. Mishustin, and W. Greiner, Phys. Rev. C **80**, 021601(R) (2009); A. B. Larionov, Nucl. Sci. Tech. **26**, S20506 (2015).
[24] J. P. Bondorf, A. S. Botvina, A. S. Iljinov, I. N. Mishustin, and K. Sneppen, Phys. Rep. **257**, 133 (1995).
[25] Z. Q. Feng and H. Lenske, Phys. Rev. C **89**, 044617 (2014); Z. Q. Feng, *ibid.* **93**, 041601(R) (2016).
[26] D. Polster *et al.*, Phys. Lett. B **300**, 317 (1993).
[27] D. Polster, D. Hilscher, H. Rossner, T. von Egidy, F. J. Hartmann, J. Hoffmann, W. Schmid, I. A. Pshenichnov, A. S. Iljinov, Y. S. Golubeva, H. Machner, H. S. Plendl, A. Grochulska, J. Jastrzebski, W. Kurcewicz, P. Lubinski, J. Eades, and S. Neumaier, Phys. Rev. C **51**, 1167 (1995).
[28] I. A. Pshenichnov, A. S. Iljinov, Y. S. Golubeva, and D. Polster, Phys. Rev. C **52**, 947 (1995).

[29] Z. Q. Feng, Phys. Rev. C **84**, 024610 (2011); **85**, 014604 (2012); Nucl. Phys. A **878**, 3 (2012); Phys. Lett. B **707**, 83 (2012).
[30] O. Buss *et al.*, Phys. Rep. **512**, 1 (2012).
[31] E. S. Golubeva, A. S. Iljinov, B. V. Krippa, and I. A. Pshenichnov, Nucl. Phys. A **537**, 393 (1992).
[32] A. B. Larionov, T. Gaitanos, and U. Mosel, Phys. Rev. C **85**, 024614 (2012).
[33] B. A. Li, A. T. Sustich, B. Zhang, and C. M. Ko, Int. J. Mod. Phys. E **10**, 267 (2001).
[34] Z. Q. Feng, Phys. Rev. C **94**, 054617 (2016).
[35] R. J. Charity *et al.*, Nucl. Phys. A **483**, 371 (1988).
[36] D. D. S. Coupland, M. Youngs, Z. Chajecki, W. G. Lynch, M. B. Tsang, Y. X. Zhang, M. A. Famiano, T. K. Ghosh, B. Giacherio, M. A. Kilburn, J. Lee, H. Liu, F. Lu, P. Morfouace, P. Russotto, A. Sanetullaev, R. H. Showalter, G. Verde, and J. Winkelbauer, Phys. Rev. C **94**, 011601(R) (2016).
[37] Z. Q. Feng, Phys. Rev. C **94**, 014609 (2016).
[38] V. Baran, M. Colonna, V. Greco, and M. Di Toro, Phys. Rep. **410**, 335 (2005).
[39] B. A. Li, L. W. Chen, and C. M. Ko, Phys. Rep. **464**, 113 (2008).
[40] Z. Q. Feng, Phys. Rev. C **94**, 064601 (2016).
[41] Z. Q. Feng, Nucl. Phys. Rev. **34**, 29 (2017).